Accepted Manuscript

Solute effects on edge dislocation pinning in complex alpha-Fe alloys

M.I. Pascuet, E. Martínez, G. Monnet, L. Malerba

PII: S0022-3115(17)30244-1

DOI: 10.1016/j.jnucmat.2017.07.049

Reference: NUMA 50421

To appear in: *Journal of Nuclear Materials*

Received Date: 25 February 2017

Revised Date: 29 June 2017

Accepted Date: 25 July 2017

Please cite this article as: M.I. Pascuet, E. Martínez, G. Monnet, L. Malerba, Solute effects on edge dislocation pinning in complex alpha-Fe alloys, *Journal of Nuclear Materials* (2017), doi: 10.1016/j.jnucmat.2017.07.049.

Solute effects on edge dislocation pinning in complex alpha-Fe alloys

M.I. Pascuet[a*], E. Martínez[b], G. Monnet[c], L. Malerba[d]

[a] *Materials Department, CONICET-CNEA – Godoy Cruz 2290 – (C1425FQB) CABA– Argentine*
[b] *Material Science and Technology Division – MST-8 – Los Alamos National Laboratory – Los Alamos – 87545 NM – USA*
[c] *EDF – R&D, MM - Avenues des Renardières - 77680 Moret sur Loing - France*
[d] *Nuclear Materials Institute, Structural Materials Expert Group – SCK•CEN – Boeretang 200 – (2400) Mol – Belgium*

ABSTRACT

Reactor pressure vessel steels are well-known to harden and embrittle under neutron irradiation, mainly because of the formation of obstacles to the motion of dislocations, in particular, precipitates and clusters composed of Cu, Ni, Mn, Si and P. In this paper, we employ two complementary atomistic modelling techniques to study the heterogeneous precipitation and segregation of these elements and their effects on the edge dislocations in BCC iron. We use a special and highly computationally efficient Monte Carlo algorithm in a constrained semi-grand canonical ensemble to compute the equilibrium configurations for solute clusters around the dislocation core. Next, we use standard molecular dynamics to predict and analyze the effect of this segregation on the dislocation mobility. Consistently with expectations our results confirm that the required stress for dislocation unpinning from the precipitates formed on top of it is quite large. The identification of the precipitate resistance allows a quantitative treatment of atomistic results, enabling scale transition towards larger scale simulations, such as dislocation dynamics or phase field.

Keywords: Iron alloys; Segregation; Edge dislocation mobility; Monte Carlo

1. Introduction

Radiation-induced hardening and embrittlement in reactor pressure vessel steels (RPV) is one of the main limiting factors for the operating lifetime of nuclear power plants. The primary mechanism at the origin of this degradation is, at the mesoscopic scale, the obstruction to the motion of dislocations by a variety of structural defects created during irradiation. While such defects are hard to observe by transmission electron microscopy (TEM), other experimental techniques such as atom probe tomography (APT) and small angle

* *pascuet@cnea.gov.ar*

neutron scattering (SANS) have evidenced the presence of Cu-rich precipitates and/or precipitates mainly rich in Mn and Ni, although containing Si, Cu and P as well [1]. Even if dislocations are in principle not directly identifiable with APT, this technique brought convincing evidence for precipitation or segregation of these solutes in their vicinity [2]. The formation of precipitates rich in Mn, Ni, Si and P close to dislocations has been observed also in low-Cu steels [3]. The presence of these precipitates clearly constitutes an obstruction to the motion of dislocations, consequently causing hardening and loss of ductility. Understanding the mechanisms involved in the latter process is thus important for the evaluation and anticipation of the lifetime of these materials when exposed to irradiation.

Thanks to the fast rising capabilities in available computing power, and also thanks to the experience gathered during recent decades of activities in the field, atomistic modelling techniques are nowadays widely employed in complement to experimental approaches for addressing this challenging goal. Previous computational studies performed by Bonny *et al.* [4], based on interatomic potentials designed with special care to describe the thermodynamics of the concerned alloys, have suggested, for instance, that at reactor operating temperature the above-mentioned solutes should preferably precipitate around the dislocation line, consistently with APT evidence. Next, the interaction with dislocation lines of dislocation loops has been studied for different solute concentrations by Terentyev *et al.* [5], concluding that Mn segregated in the core of loops causes an increment in the yield point and finally increases the hardening. P is also known to segregate to heterogeneities in RPV steels, mainly grain boundaries and dislocations, causing embrittlement, grain boundary de-cohesion and thereupon a shift in the ductile-to-brittle transition temperature [6-7].

The objective pursued in this work is to provide a better understanding of the role played by solute segregation in the pinning of dislocation, focusing on the case when the precipitates decorate or contain the dislocation line, before load is applied, rather than being approached and sheared by a moving dislocation. This is a challenging objective because of the inherent multiscale aspect of the problem, and the unavoidable necessity to consider reference configurations with many hundreds of thousands of atoms at the very least. To address it adequately, two atomistic modelling techniques available in the LAMMPS code [8] are used in complement to each other during two separate steps, as briefly described in what follows. (*i*) To start with, representative configurations for the alloys of interests in which solutes decorate dislocation are investigated, using interatomic potentials of proven validity. For this purpose, solute precipitates and segregation profiles in thermal equilibrium near edge

dislocations are obtained with an atomistic Monte Carlo (MC) method in the variance-constrained semi-grand-canonical (VC-SGC) ensemble, as proposed by Sadigh *et al*. [9]. More explicitly, we henceforth denote it as Molecular Dynamics – Monte Carlo (MD-MC), in reference to the synergy that it operates between these two classical methods. It is important to emphasise from the start that this is a method that seeks for configurations of minimal free energy, but does not provide any information about the kinetics of the process: MD samples the vibrational degrees of freedom at a given temperature. It thermalizes the system in the energy minimum. This MD-MC approach has the great advantage to be fully applicable for multicomponent systems containing millions of particles, yet being easily parallelized in an efficient way amongst many processors. The latter quality would, unfortunately, be rather hard to achieve for other, more general purpose and less customized algorithms strictly working on the canonical (CS) ensemble. On the other hand, classical semi-grand-canonical (SGC) ensemble approaches are easily parallelized, but are inapplicable to study precipitation. (*ii*) From the atomic configurations obtained during the previous step, classical MD, this time as a kinetic method, is then applied at various temperatures, in order to get the stress-strain curve while applying an external shear load. The purpose of the latter is, quite clearly, to induce the motion of the dislocation, thereby simulating an external load applied at the macroscopic scale. For the sake of completeness, it is worth at this stage noting that the so obtained stress-strain curve is a localized measurement of hardening, but does not bring a direct estimation for it at the macroscopic scale. It rather serves as input for larger scale modelling techniques such as dislocation dynamics, devoted to formally estimate the resulting hardening.

The paper is organized as follows. First, the two above-mentioned atomistic modelling techniques, on which the work is based, are briefly described in section 2, summarizing the most important information for the unfamiliar reader. Next, our results are thoroughly presented in section 3. This section is naturally divided in two complementing parts. In the first one, solute segregation in presence of the edge dislocation BCC Fe is studied with MD-MC for three representative systems in connection with RPV steels, namely: FeCuNiMn, FeNiMn and FeP at 300K, and 500-550K. The corresponding stress-strain curves are then reported in the second part. Available embedded atom method (EAM) interatomic potentials are used to model the interactions in all systems. Discussions and conclusions constitute the closing section 4.

2. Methods

As already explained, our work has been performed with the combination of two complementing modelling techniques implemented in the LAMMPS code [8]. First, the so-called MD-MC approach is used to get relevant reference configurations, as described in section 2.1. Next, classical MD is applied to get the stress-strain curves, as described in section 2.2.

2.1 Thermodynamic modelling with the MD-MC technique

Solute precipitation by minimizing the free energy of the system has been simulated by an MD-MC hybrid algorithm in the VC-SGC ensemble [9]. This method is suitable to simulate systems with millions of particles in the whole concentration range. Chemical mixing, precipitation, relaxation and thermal vibrations, as described by the interatomic potentials, are taken in account by the combination between transmutation moves and MD steps used for relaxation. However, the model does not provide any information on kinetics, i.e. diffusion processes that would take prohibitively long computational time are not considered. The Monte Carlo tries to take the system to the right distribution in compositional space. That is, the probability of each state will comply with a Boltzmann distribution. Specifically, in the SGC ensemble the phases inside the miscibility gap have identical chemical potentials and therefore the concentration cannot be held constant, so the nature of specific atoms changes while the energy minimization proceeds. Outside the miscibility gap, the chemical potential defines the equilibrium concentration. The partition function of the semi grand-canonical ensemble is:

$$Z_{SGC}(\Delta\mu, N, V, T) = \int_0^1 Z_C(c, N, V, T) \exp[-\beta \Delta\mu N c]\, dc \qquad (1)$$

where $\beta = 1/k_B T$, N is the number of particles, c is the concentration and Z_C is the partition function of the canonical ensemble. To be able to study segregation at a constant concentration inside the miscibility gap and maintain computational efficiency, a new equilibrium ensemble (VC-SGC) was developed, by adding a new constraint to the statistical mechanics derivation of the equilibrium on the average squared concentration $\langle \hat{c}^2 \rangle$. This ensemble has two independent parameters, ϕ and κ, associated with constraints on the first

and second moments of the concentration (the statistical mechanical origin is described in [9]). The partition function of this VC-SGC ensemble is:

$$Z_{VC-SGC}(\phi, \kappa, N, V, T) = \int_0^1 Z_C(c, N, V, T) \exp[-\beta\phi(Nc) - \beta\kappa(Nc)^2]\, dc \qquad (2)$$

Similarly to the SGC ensemble, the MC is performed following the scheme given by: *i*) select one particle at random, *ii*) change its chemical identity and *iii*) calculate the energy change ΔU and c the concentration change Δc. Finally, the acceptance probability is given by:

$$A = min\{1, exp[-\beta(\Delta U + N\Delta c(\phi + 2N\kappa c))]\} \qquad (3)$$

The force associated with a change in the chemical type (acceptance probability of one event) receives contributions from both the change of energy ΔU as well as the external concentration dependent force $N\Delta c(\phi + 2N\kappa c)$. Comparing with the SGC ensemble, the change in the chemical potential now becomes:

$$\Delta\mu = \phi + 2N\kappa c \qquad (4)$$

In practice, κ is taken from [9] and controls the fluctuations around the desired concentration. ϕ is chosen such that the system is driven inside the miscibility gap with a tuned thermodynamic driving force, to optimize the acceptance probability along the whole simulation. The MC method is applied for transmutation together with MD, that is used to obtain better system relaxations.

The interaction for the ternary FeNiMn and the quaternary FeCuNiMn systems are modeled using the EAM interatomic potential proposed by Bonny *et al.* [10], while the FeP system has been modeled using the EAM interatomic potential developed by Ackland *et al*. [11]. Together, this is the closest one can get to simulate RPV steels with available interatomic potentials, given that no potential exists for the 6-nary alloy FeNiMnCuSiP, nor for any other quaternary alloy different from FeNiMnCu.

One sample with a dipole of edge dislocations is generated using linear elasticity [12] in a crystallite with the normal axes *x*, *y* and *z* oriented as the $[1\bar{1}0]$, $[111]$ and $[\bar{1}\bar{1}2]$ directions, that contains approximately $6{\cdot}10^5$ atoms of Fe-bcc. The Burgers vectors of the dipole are $\mathbf{b}_1 = a_0/2\ [111]$ and $\mathbf{b}_2 = a_0/2\ [11\bar{1}]$, where a_0 is the lattice parameter of Fe [4-13].

The presence of the dipole allows periodic boundary conditions to be applied in all directions. The dimensions of the box are 28 x 30 x 10 nm and are sufficient to ensure that the dislocation lines, both lying along the $[\bar{1}\bar{1}2]$ direction, are well-separated from each other to prevent their mutual interactions. The $\Delta\mu$ used are: -0.69 for Cu, 0.29 for Ni, -1.38 for Mn and -2.06 for P, with $\kappa = 1000$ in all cases. These values drive the system into the miscibility gap and constrain it to sample configurations with the required concentration in each case. Once these values are fixed, 500 MD relaxation steps are performed between MC steps, decreasing the free energy of the system to achieve the desired concentrations: 1%Ni-1%Mn, 0.7%Ni-1.4%Mn, 0.5%Cu-1%Ni-1%Mn, 0.5%Cu-0.7%Ni-1.4%Mn and, in the case of P, from $8.3\ 10^{-3}$ % to $2.83\ 10^{-2}$ %. The temperatures considered are: 300K and 500K-550K (inside the miscibility gap and below or slightly below normal reactor operating temperatures).

The reason to choose these initial compositions is because, except for Cu, they correspond to the solute content of RPV steels representative of those used in nuclear power plants operating in France and Germany, for which, moreover, experimental data from microstructural examination and mechanical characterization after irradiation are widely available, so that they were used as reference materials in the framework of the FP7 PERFORM60 project [14]. Table 1 shows an example of composition of these steels. The Cu content is artificially high in order to have sufficient precipitated Cu to be able to see the difference, if any, between Cu presence or absence. The two temperatures have been chosen based on the following reasoning. 300K is essentially room temperature and, although materials in a reactor are exposed to much higher temperature, it is an obvious reference case to be chosen, at which typically irradiations with ions or electrons are performed. 500 and 550K are chosen for being as close as possible to the operating temperature of RPV steels (563K), but low enough to ensure that, with the potential used, precipitation would occur for the compositions chosen, based on the study performed in [4]. As a matter of fact, the objective here is to obtain solute configurations that should mimic as much as possible those that APT would be expected to observe around dislocations, as a consequence of precipitation or segregation induced by irradiation. The method we use leads by definition the system towards thermodynamic equilibrium. In equilibrium, according to the potential used, no or only very little precipitation would occur at 563K. However, under irradiation out of equilibrium processes take place as well, in particular dragging of solutes by point-defects [15], that lead to segregation and precipitation also at temperatures above the miscibility gap, where precipitation is not thermodynamically favourable. Moreover, the steels are complex

alloys that contain also other elements, e.g. Si, that may influence the equilibrium itself, enhancing thermodynamically driven precipitation. Thus, producing the reference configurations at 500K (in FeMnNi alloys) and at 550K (in FeMnNiCu) alloys corresponds to the closest we can get to realistic conditions, given the limitations of the methodology applied. In the case of P, in contrast, that can only be studied separately because of the lack of potentials that include it with other elements, the concentrations are low because this element is always present in very low concentration in steels. The configurations obtained are hence not expected to perfectly mirror the real ones but, at least, they are going to be plausible and, importantly for the stability of the system, they are in equilibrium with the presence of the dislocation.

Table 1: Chemical composition of 20MnMoNi5 5 [weight %] (M1), and chemical composition of S3NiMo1/OP41 TT [weight %] (M2) [14].

	C	Si	Mn	P	S	N2	Ni	Cr	Mo	Al	V	Ta	Cu	Co
M1	0.183	0.27	1.373	0.007	0.0083	0.01	0.793	<0.1	0.483	0.18	0.12	<0.01	0.05	0.015
M2	0.05	0.123	1.08	0.0186	0.0093	0.01	1.013	<0.1	0.616	0.012	0.0113	<0.01	0.03	0.0096

2.2 Stress-strain curve calculation with MD

Once the equilibrium configurations have been obtained, simple shear is applied in a classical MD simulation at a constant 10^9 s^{-1} strain rate, at 300 and 600K. These are representative temperatures, at which typically tensile tests are performed (room temperature and irradiation temperature, or somewhat above), that have been used also in previous simulation work addressing the interaction of dislocations with radiation defects [5]. For better computational efficiency, only half of the sample is used, which contains a single dislocation.

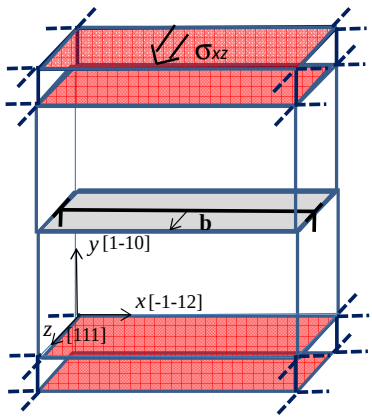

Figure 1: Schematic representation of the box containing edge dislocation with **b** = [111].

The dislocation density is then 25 10^{14}m^{-2}. Two atomic layers of 12 Å thickness, parallel to the dislocation glide plane, i.e. normal to the *y* axis, are fixed, as shown in Fig.1. Periodic boundary conditions along [111] and $[\bar{1}\bar{1}2]$ (*x* and *z*) are applied. Shear strain is applied by displacing the upper layer of the simulation box in the direction of the Burgers vector and the corresponding resolved shear stress induced by the applied deformation is calculated as $\sigma_{xz} = F_z/A_{xz}$, where F_z is the total force in the *z* direction and A_{xz} is the *xz* cross section area [16].

3. Results

3.1. Solute precipitation around the edge dislocation

In all cases studied in this work, heterogeneous segregation to the dislocation core is observed, consistently with [4], where the influence of the presence of dislocations on the local solubility limit was studied. Representative cases are shown in Fig.2: (*a*) Fe-0.7%Ni-1.4%Mn and (*b*) Fe-0.5%Cu-1%Ni-1%Mn obtained at 300K, in which almost all the solutes precipitate; (*c*) Fe-1%Ni-1%Mn at 500K and (*d*) Fe-0.5%Cu-0.7%Ni-1.4%Mn at 550K, where only a fraction of the solutes precipitate. This is consistent with the phase diagram, where the solubility limit increases with increasing temperature, and therefore less solutes precipitate.

3.1.1. *Iron-nickel-manganese*

At 300K almost all the solutes precipitate in all the alloys studied (one case as example is depicted in Fig.2.*a*), meaning that at this temperature the solubility limit according to the potential is virtually zero, or anyway very low. At 500K, in contrast, in the Fe-1%Ni-1%Mn alloy only 0.64%Ni and 0.86%Mn (73.18% of the total) precipitate (see Fig.2.*c*), while in the Fe-0.7%Ni-1.4%Mn alloy, only 0.29%Ni and 1.35%Mn (75.85% of the total) precipitate, both in the dislocation line zone. The clusters' shape is nearly spherical, in agreement with the simulations performed in Bonny *et al.* with a different MC method [4]. The shape departs from spherical along the dislocation because of the coalescence of separately nucleated spherical precipitates. In the FeMnNi alloys, like in previous work using MC in the isothermal-isobaric (N,P,T) ensemble, the presence of dislocations increases

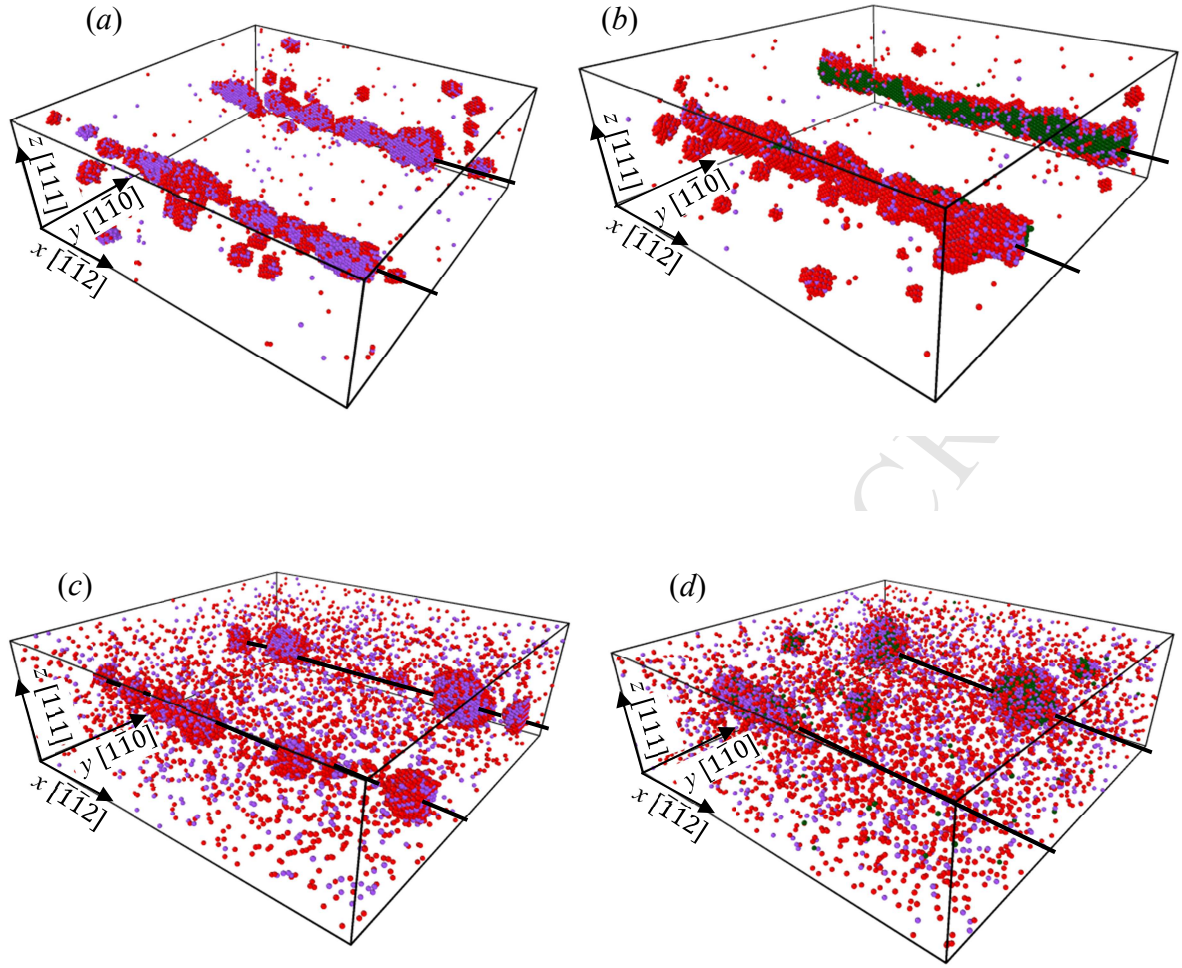

Figure 2. Distribution of solutes in presence of an edge dislocation dipole. (*a*) Fe-0.7%Ni-1.4%Mn segregation temperature: 300K, (*b*) Fe-0.5%Cu-1%Ni-1%Mn segregation temperature: 300K, (*c*) Fe-1%Ni-1%Mn segregation temperature: 500K and (*d*) Fe-0.5%Cu-0.7%Ni-1.4%Mn segregation temperature: 550K. Ni atoms in red, Mn atoms in violet and Cu atoms in green. Dislocation lines are denoted by a black line.

significantly the thermal stability of the intermetallic phase MnNi (B2), as well as of Mn precipitates. Such clusters are attached to dislocation lines, depending on the alloy composition. In the cases with more Mn than Ni solutes, the visible result is that Mn atoms precipitate in the core, increasing the size of the precipitate, while the intermetallic phase MnNi always forms around the precipitated Mn, suggesting that the interface energy between the B2 phase and Fe is lower than the one between pure Mn and Fe, at least according to the interatomic potential. A transversal *xz* section of the simulation box is shown in Figs. 3.*a* and 3.*b*, where it is possible to appreciate the solute distribution around the dislocation.

3.1.2. *Iron-copper-nickel-manganese*

As in the previous alloys, at 300K complete precipitation at the dislocation core is observed (one case as example is depicted in Fig.2.*b*). In contrast, at 550K, for the Fe-0.5%Cu-1%Ni-1%Mn alloy, only 0.29%Cu, 0.64%Ni and 0.61%Mn (45.32% of the total) precipitate in the dislocation line zone. In the Fe-0.5%Cu-0.7%Ni-1.4%Mn alloy, only 0.39%Cu, 0.15%Ni and 1.13%Mn (51.32% of the total) precipitate in the dislocation line zone (Fig.2.*d*). The precipitate composition is sensitive to the composition of the alloy and the temperature, as studied in [4]. In the FeCuNiMn alloys, Cu atoms precipitate in the tensile region of the core, while pure Mn atoms precipitate mainly in the compressed zone of the core, with the intermetallic NiMn phase surrounding the Mn atoms, again in agreement with Bonny *et al.* [4], and suggesting little affinity between Cu and Mn. In fact, the precipitation of Cu reduces the amount of precipitated Mn, as well as, to a lesser extent, Ni. The transversal *xz* section (Figs.3.*c* and 3.*d*) shows an analysis of the precipitate content and the distribution of them around the dislocation line. The precipitation in this quaternary alloy is explained in [4]. The radiation defects have a strong influence on the precipitate stability, increasing the phase stability limit. At reactor operating temperature, solutes can thus favourably segregate at the dislocation, but this would not happen in the absence of lattice defects, i.e. only heterogeneous nucleation or out of equilibrium segregation may occur at reactor operating temperatures. The precipitate composition is then obviously sensitive to both the composition of the alloy and the temperature.

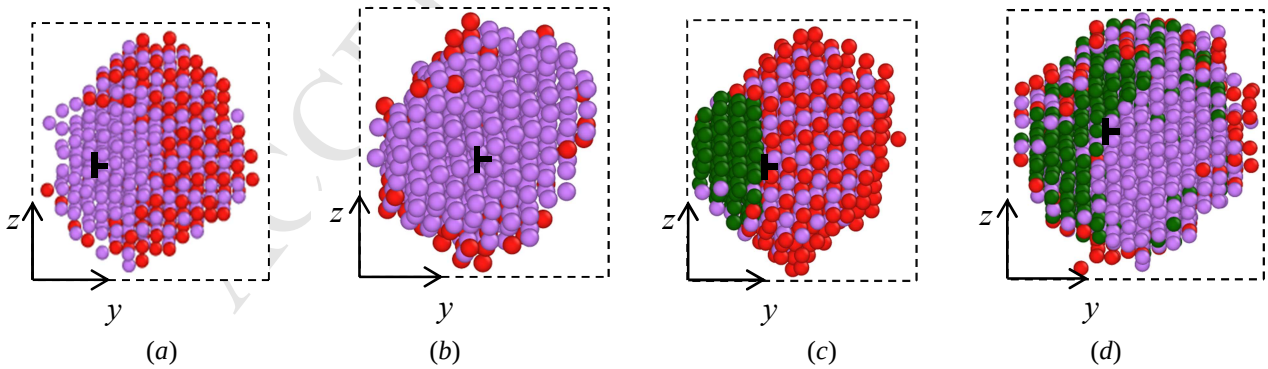

Figure 3: Cluster sections of representative examples on: (*a*) Fe-1%Ni-1%Mn at 500K, (*b*) Fe-0.7%Ni-1.4%Mn at 300K, (*c*) Fe-0.5%Cu-1%Ni-1%Mn at 300K and (*d*) Fe-0.5%Cu-0.7%Ni-1.4%Mn at 550K. Green atoms: Cu, red atoms: Ni and violet atoms: Mn. Dislocation line in black.

3.1.3. *Iron-Phosphorus*

We have also studied the segregation of P to the core of an edge dislocation in α-Fe at 300K. We observe a strong segregation of the P atoms to the dislocation core, mostly to the compressive side of the dislocation. Since P is present only in a small quantity, no precipitation occurs, not even close to the dislocation line. Thus, one should mainly interpret the results in terms of affinity of single P atoms for the dislocation line. The binding energy of a single P atom to the dislocation core is E_b=-0.54 eV, which represents a significant driving force for P to segregate. On the other hand, on the tensile side there are sites with substantial repulsion that might reach E_b=1.5 eV. Therefore, depletion of P is expected on that side. The binding energy was calculated as the difference between the energy of the system with a P atom at the most favorable site at the dislocation core and the energy of the system with the P atom in a region of the sample representative of bulk (i. e. far from the dislocation). Note that a positive binding energy represents a repulsive interaction while negative implies attraction. It is worth noting that the Fe-P interatomic potential does not describe the P-P interactions correctly, as pure P is covalently bonded. This is an additional reason to use only small concentrations of P in the simulations. Although the local concentration increases at the dislocation core, the P-P component of the interaction remains low compared to the Fe-P, therefore we may consider the bias acceptable.

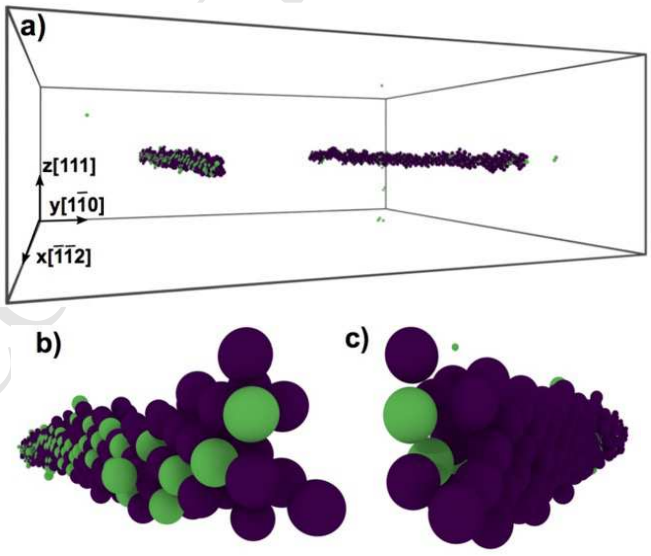

Figure 4. Distribution of P atoms (green) in the presence of an edge dislocation dipole in α-Fe (blue). The P concentration is 0.03%. (*a*) shows the box orientation with the dislocation dipole and (*b*) displays a zoom into the compressive side of one of the dislocation cores. (*c*) displays a zoom into the tensile side of the same dislocation core as *b*).

3.2. Effect on mobility of edge dislocations

3.2.1. *Iron-manganese-nickel and iron-copper-manganese-nickel*

Once the configurations described above have been obtained by MC simulations, the samples are divided in two parts, each one containing only one dislocation. In the samples obtained at 300K, where precipitation is complete, solutes precipitate in equal amounts around both dislocations of the dipole. In the case of the alloys obtained at 500 and 550K, in contrast, the final concentration of Cu, Ni and Mn around each dislocation is not necessarily the same: the solubility limit is correct if the whole sample is considered, but locally there are differences. Thus, we effectively obtained samples (half-samples) with overall concentrations that are different from the initial one. This is actually an advantage, because it allows us to explore more cases. The alloys chosen to which the strain is applied are thus: Fe-1%Ni-1%Mn, Fe-0.5%Cu-1%Ni-1%Mn, Fe-0.7%Ni-0.8%Mn, Fe-0.7%Ni-2%Mn and Fe-0.4%Cu-0.6%Ni-0.9%Mn (an Fe-0.6%Cu-0.8%Ni-2%Mn sample was set aside because the precipitate on the dislocation line was too large to avoid boundary effects). We have therefore studied the dislocation unpinning in the samples listed above at the two temperatures representative of tensile test temperatures: 300K and 600K. The unpinning stress for segregation obtained at a temperature of 300K for the different alloys are near 2000MPa (see Table 2), which is way too high to allow any dislocation motion. This suggests that *edge dislocation segments are practically immobile under usual deformation conditions when they are fully surrounded by stably segregated or precipitated solutes*. These values are interpreted in the Discussion section (see below).

Table 2: Composition of precipitates (%) after segregation at 300K, volume fraction of B2 precipitates (%), volume fraction of total precipitates (%), maximum shear stress (MPa) obtained at MD simulations at 300 and 600K. (Tiny numbers of Mn, Ni or Cu atoms are left in the matrix).

Alloy	Comp. of precipitates (%)			B2 frac.	Total frac.	Max. stress	
	Cu	Ni	Mn			600K	300K
1%Ni-1%Mn		45.7	54.3	0.0081	0.0177	1538	1804
0.7%Ni-1.4%Mn		25.6	74.4	0.0040	0.0158	1120	1417
0.5%Cu-0.7%Ni-1.4%Mn	21.4	20.6	58.0	0.0046	0.0224	1656	1932
0.5%Cu-1%Ni-1%Mn	19.3	39.0	41.7	0.0078	0.0200	2100	2365

Focusing now on the configurations obtained at segregation temperatures of 500K and 550K, the stress-strain relationships at 300K are shown in Fig.5 for the Fe-1%Ni-1%Mn alloy. Different views of the dislocation movement are shown too, obtained with the so-called *Dislocation Extraction Algorithm* (DXA), a computational method developed by the authors of OVITO [17-18]. Since precipitates around the dislocation line are strong obstacles, the dislocation segments inside the precipitates are strongly pinned. Given their small length, the free segments start to bow out at high stress, as can be seen in Fig.5. At this high stress, two free dislocations segments start to bow out around the spherical precipitate in the left-half of Image *b* (Fig.5). The curvature increases tremendously the effective stress (local stress) on the pinned segment inside the precipitate [19]. When the stress exceeds 800 MPa, the precipitate can no longer sustain the effective stress and the pinned segment is released, sweeping a large

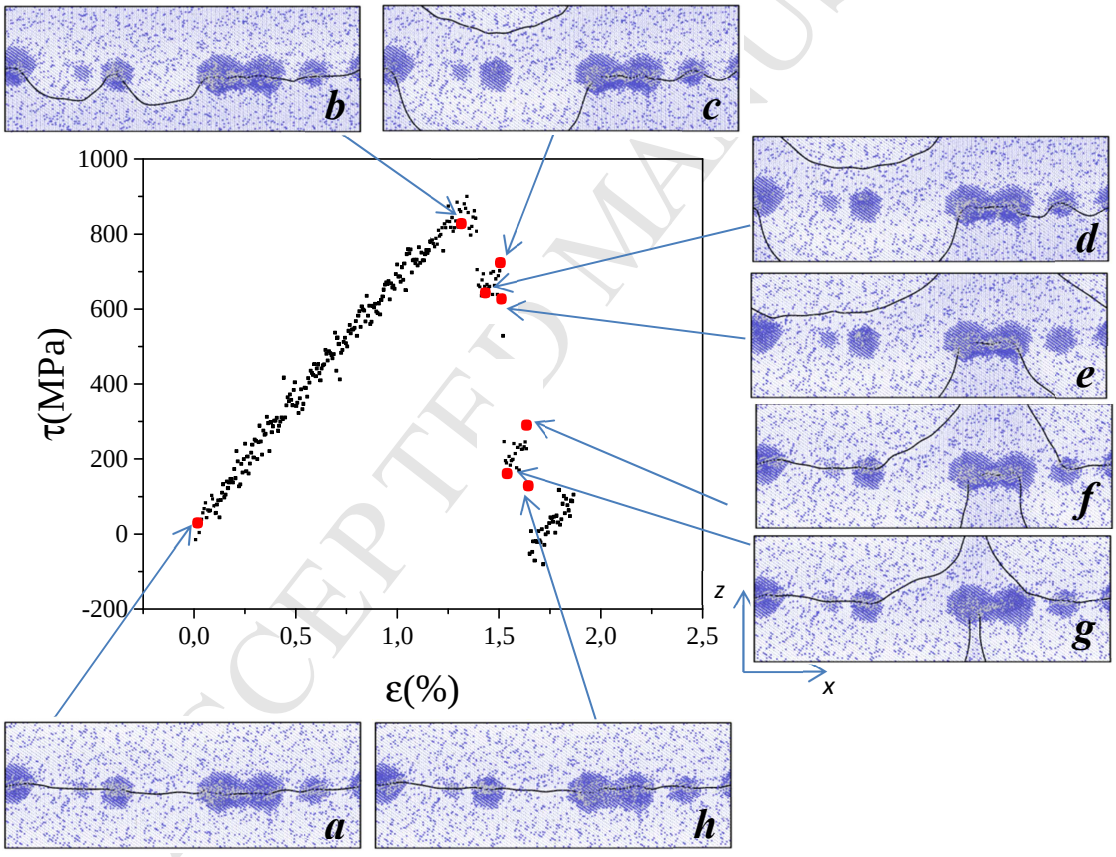

Figure 5: Stress-strain relationship at stress-strain temperature: 300K corresponding to the interaction of an edge dislocation ½ ⟨111⟩ {110} in a Fe box with 1%Ni-1%Mn. Different views of the dislocation movement are shown. (Segregation temperature: 500K).

area (Image *c*). The resulting plastic deformation results in an important elastic relaxation, which leads to a significant stress drop. Then the dislocation unpins from the precipitate on the border of the simulation box (Image *d*) leading to further relaxation. Unpinning from the two close precipitates (Image *g*) operates only when the dislocation re-enters the simulation box from the upper side, which is an artifact due to the periodic boundary conditions.

A detailed comparison of the loading curves over the different configurations is presented in Fig.6 for temperatures: 300K (*a*) and 600K (*b*). The shape of the curves at 300K and 600K are similar, only the unpinning stress changes, with higher values corresponding to 300K. To compare with a system without clusters, a reference curve (friction stress) is also shown, obtained with random distribution of solutes at the same concentrations. Because the friction curves are similar, only one is shown for clarity (Fe-0.5%Cu-1%Ni-1%Mn). Table 3 summarizes the main results in terms of maximum stress and depending on the concentration of Cu, Ni and Mn.

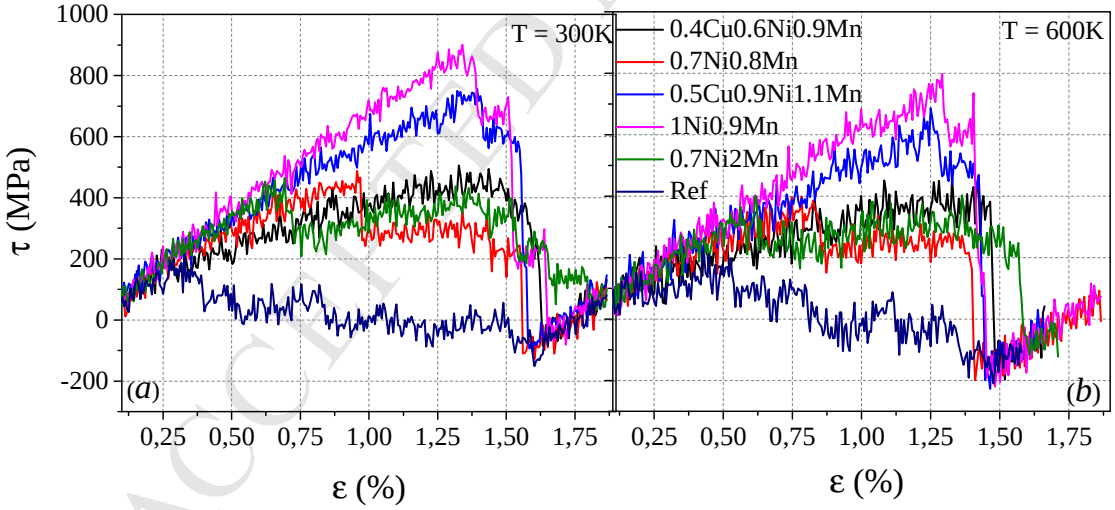

Figure 6. Stress-strain curves for an edge dislocation in BCC Fe with different concentrations of CuNiMn (segregation temperature: 500K and 550K). The composition of the alloys and the temperature are reported in the figure.

Table 3: Composition of precipitates near dislocation line (%) and in the matrix after segregation at 500 or 550K, percentage of solutes in matrix, volume fraction of B2 precipitates (%), volume fraction of total precipitates (%) and maximum shear stress (MPa) of loading at 300 and 600K.

Alloy	Comp. of precipitates (%)			Solutes in matrix (%)			B2 frac.	Total frac.	Max. stress	
	Cu	Ni	Mn	Cu	Ni	Mn			600K	300K
1%Ni-1%Mn		46.0	54.0		0.07	0.17	0.0061	0.0133	798	900
0.7%Ni-0.8%Mn		23.9	76.1		0.42	0.11	0.0023	0.0097	398	488
0.7%Ni-2%Mn		15.1	84.9		0.40	0.11	0.0035	0.0234	401	465
0.4%Cu-0.6%Ni-0.9%Mn	26.8	9.7	63.5	0.17	0.57	0.29	0.0009	0.0095	457	505
0.5%Cu-1%Ni-1%Mn	26.7	16.2	57.1	0.12	0.72	0.37	0.0021	0.0128	686	757

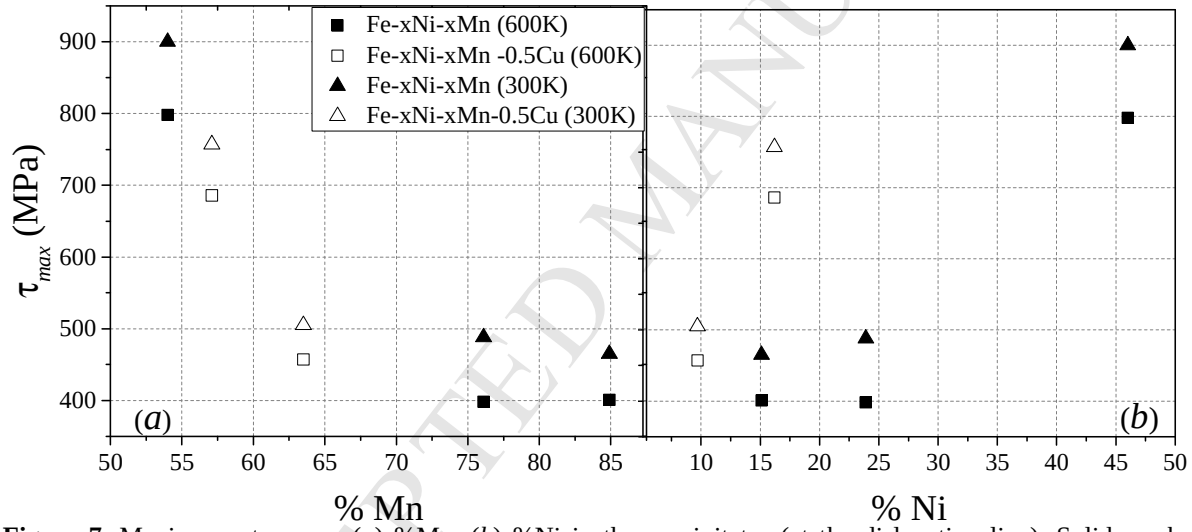

Figure 7. Maximum stress vs. (*a*) %Mn, (*b*) %Ni in the precipitates (at the dislocation line). Solid symbols correspond to alloys without Cu atoms, empty symbols correspond to alloys with 0.5% Cu. Triangles and squares show results at 300K and 600K, respectively. (Segregation temperature: 500-550K).

Fig.7 shows precipitation unpinning stress for the cases depicted in Table 3 as a function of (*a*) Mn concentration and (*b*) Ni concentration in the precipitates near the core. While the unpinning stress decreases with the amount of Mn, it increases with the amount of Ni, consistently with the observation made in Bonny *et al.* [4]. Ni atoms are found to be preferably diluted in the matrix and not to form isolated clusters. Instead, they enter to form the ordered B2 structure together with Mn atoms that surround the pure Mn clusters. Fig.7 thus suggests that this structure is harder than pure Mn, its volume fraction being proportional to the amount of Ni. So the unpinning stress effectively increases when the fraction of B2

phase increases. This suggestion is broadly confirmed by Fig.8.*a*, that shows how, in all cases (including when the precipitation has been simulated at segregation temperature equal to 300K), the unpinning stress increases with the amount of B2, although clearly also other variables play a role. For example, the Cu content in the clusters, which does not affect much the quantity of segregated Mn atoms, but reduces the amount of Ni, reduces the fraction of precipitated B2. However, the presence of Cu, for similar fractions of precipitated B2 phase, has the effect of increasing the total unpinning stress (the empty symbols in Fig.8.*a* lie above the full symbols). This suggests that the total volume fraction of precipitates is also a variable influencing the hardening. Fig.8.*b* shows that indeed there is a trend for the unpinning stress to increase with the increasing volume fraction of precipitates. Yet, even this variable is insufficient, by itself, to explain the hardening. In the discussion section the influence of the distribution of precipitates is analysed and used to rationalize in a generalized way the effect on hardening of precipitation on dislocations.

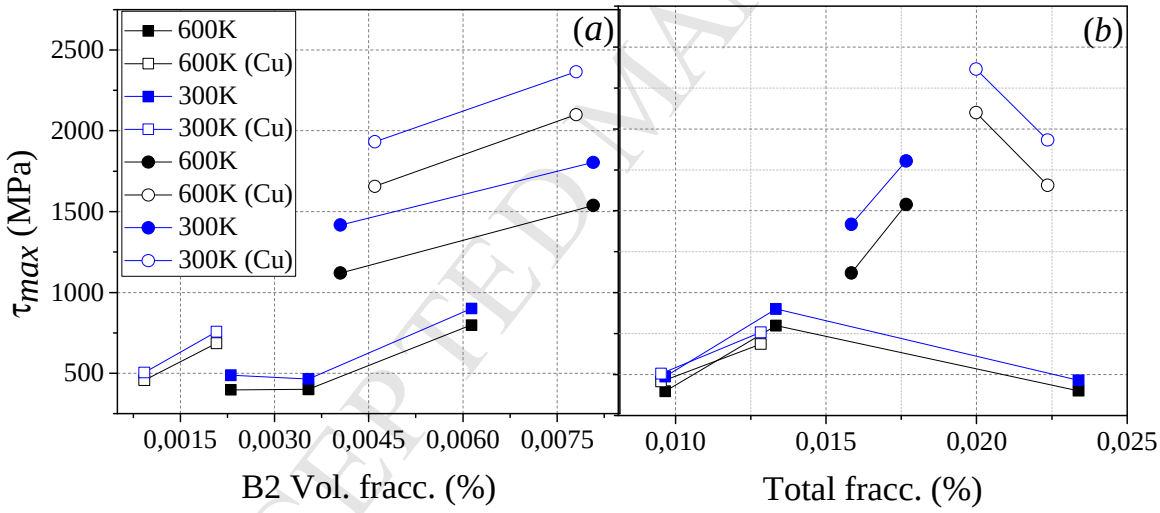

Figure 8. Maximum stress vs. (*a*) volume fraction of precipitated B2 phase (*b*) total volume fraction of precipitates (in both cases at the dislocation line). (Values from tables 1 and 2). Solid symbols correspond to alloys without Cu atoms, empty symbols correspond to alloys with 0.5% Cu. Squares (circles) show results at 300K and 600K, respectively samples have been obtained at segregation temperature: 500 and 550K (Segregation temperature: 300K).

3.2.3 *Iron-phosphorus*

The same methodology has been followed to analyze the effect of P segregation on the response of the material to external loading. Simple shear was applied on the samples with different P content. The resulting stress-strain curves are shown in Fig.9.*a*, where it is observed that, despite its small concentration, the presence of P significantly increases the yield point, leading therefore to hardening. For non-interacting particles, the extra work to be performed on the material for the dislocation to overcome the obstacle is directly proportional to the binding energy of a single atom into the dislocation core, multiplied by the number of atoms [20].

$$\sigma b \cong \frac{c_d E_B}{b} \tag{5}$$

Where σ is the yield stress, b is the Burguer vector, c_d is the linear concentration of solutes along the dislocation line and E_B is the binding energy. Fig.9.*b* shows the dependence of the unpinning point with the amount of P. For small P contents we observe that the results follow a straight line with slope given by the binding energy, as predicted by theory. The slope found from the fitting is 0.15 eV, which is in very good agreement with the averaged 0.21 eV of the binding energy at attractive sites. In the Monte Carlo calculation not all the P atoms are in the most favorable sites due thermal fluctuations. Thus, the deviation from the calculated value is to be expected. As the P concentration increases, the results deviate from the straight line,

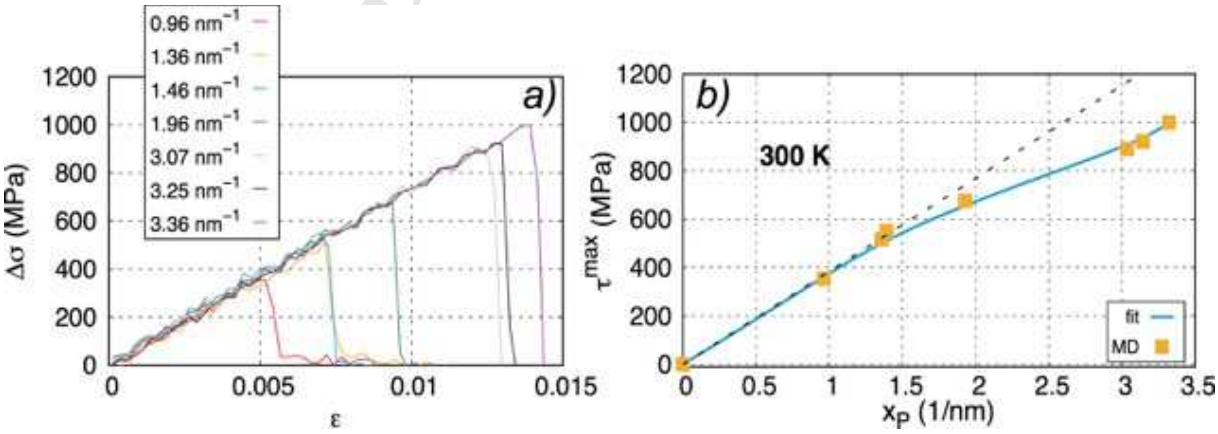

Figure 9. (*a*) Stress-strain curves depending on the P content. (*b*) Yield stress versus P composition. Yellow points represent MD results and the blue line shows a spline fit. The dashed straight line displays a slope given by the binding energy of a single P atom to the edge dislocation.

because P-P interactions start to play a role. It is worth mentioning that is a general trend and the linear relation is not valid solute-solute interactions are significant. As stated above, the interatomic potential used in these calculations does not reproduce satisfactorily the P-P interaction, so these points have to be taken with care.

4. Discussion

In the Fe-Ni-Mn ternary and Fe-Cu-Ni-Mn quaternary alloys, solute precipitation to the core of dislocations occurs fully at 300K and partially at 500K and 550K. Mn and Ni segregate largely to the dislocation core. The precipitates might exhibit a core shell structure, depending on the concentration of each element, with pure Mn at the core and a MnNi intermetallic with the B2 crystalline structure in the outer region. Cu atoms occupy competing positions in the dislocation core, meaning that the addition of Cu suppresses the precipitation of Ni and Mn to the core. This result can be explained by elasticity theory considerations, comparing the lattice parameters of the different precipitates phases: bcc Mn and B2 NiMn are undersized compared with bcc Fe, while bcc Cu is oversized, in concordance with results published by Bonny *et al*. [4].

Despite the clear stronger hardening effect of the B2 phase, here we shall analyse the results without distinguishing between precipitate composition, focusing only on the shape and distribution of the precipitates along the line, both in the case of FeMnNi(Cu) (Fig.8.*a*) and of FeP (Fig.9.*a*). However, Fig.8 suggests that the precipitate volume fraction is not sufficient, alone, to explain the strengthening and other variables play a role, as well. In order to quantify the pinning effect of the dislocation motion, we therefore interpret the MD simulation results on the basis of the method reported by Monnet *et al.* [21,22]. In this method, the pinning is characterized by the local stress necessary for a dislocation segment to penetrate and shear the precipitate. It is equivalent to a “friction” stress inside the precipitate and is called precipitate resistance τ_{obs} in the following. Based on previous work [21,22], this resistance, that affects only the segment of dislocation inside the precipitate, is on the order of a GPa. The objective of the present discussion is to estimate this precipitate resistance as a function of composition and temperature. However, the original method was designed to estimate the resistance from MD simulations of a dislocation interacting with a periodic row of identical precipitates (periodic boundaries were used). A slight modification has to be

considered because in the configurations tested in this work, not only one precipitate is pinning the dislocation but several ones.

Let us consider unpinning from a precipitate "p" of size D in the middle of Fig.10. Two segments of length l_1 and l_2 are bounding P (see Fig.10).

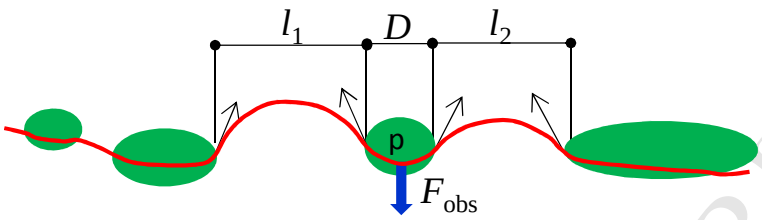

Figure 10: Schematic configuration of dislocation unpinning from precipitate *p*.

They experience two applied forces ($\tau_a b l_1$) and ($\tau_a b l_2$). Since every bowing segment is pinned by two precipitates, precipitate P experiences one half of ($\tau_a b l_1$) and one half of ($\tau_a b l_2$). In addition, P is subject to the applied force ($\tau_a b D$) on the dislocation segment of length D that is going to shear it. At the unpinning applied stress τ_{max}, precipitate P is thus subject to a total driving force F_{max} = [½ (l_1 + l_2) + D]$b\,\tau_{max}$, which must be balanced by the pinning force F_{obs} = $Db\,\tau_{obs}$. Consequently, the obstacle resistance can be obtained as:

$$\tau_{obs} = \frac{l_1 + l_2 + 2D}{2D}\tau_{max} \qquad (6)$$

Four simulations were used to estimate the obstacle resistance. The configurations are shown in Fig.11. In order to avoid the periodic boundary artefacts, unpinning must occur before any dislocation segment leaves the simulation box and re-enters it from the opposite face.

Unfortunately, this condition could not be satisfied in the case of 0.4%Cu-0.6%Ni-0.9%Mn alloy. The precipitate size and the lengths of the dislocation segments to the left and to the right of the indicated precipitates have been computed for MD simulations performed at 300 and 600 K. When plotting τ_{max} as a function of [$2D$/ (l_1 + l_2 + $2D$)] the slope indicates the precipitate resistance τ_{obs}. Results are shown in Fig.12, where simulations at 300 K are plotted

in circles and those at 600 K in rectangles. As can be seen from the figure, data are aligned along straight lines passing by zero. The slope of the line at 600 K is slightly less than that at 300K. This indicates that precipitates in all alloys can be characterized by a similar resistance of 2400 MPa at 300 K and 2100 MPa and 600 K.

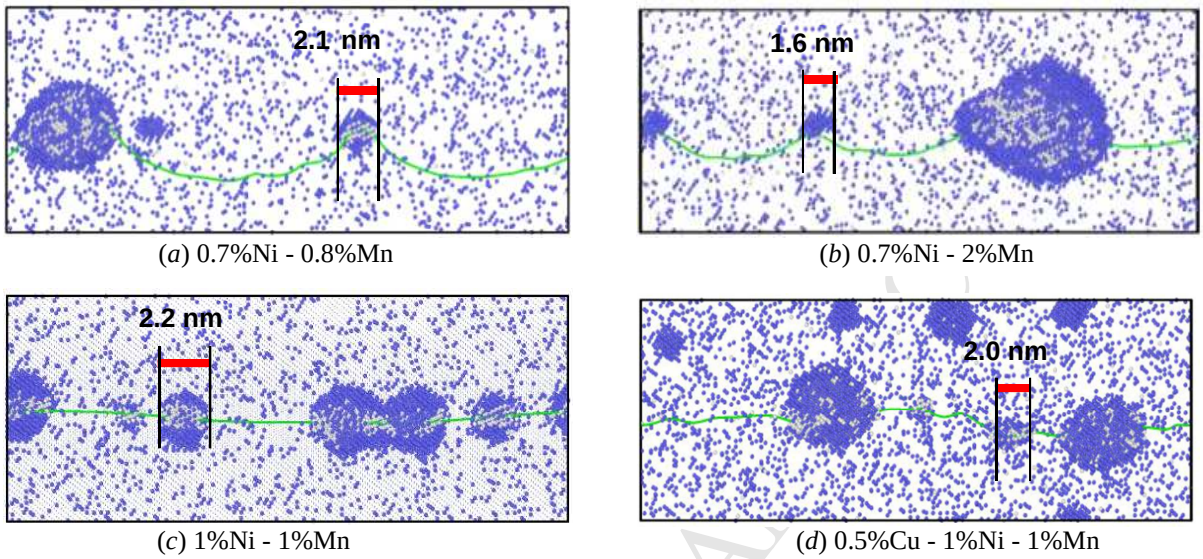

(*a*) 0.7%Ni - 0.8%Mn (*b*) 0.7%Ni - 2%Mn

(*c*) 1%Ni - 1%Mn (*d*) 0.5%Cu - 1%Ni - 1%Mn

Figure 11: MD configurations used to compute the precipitates resistance. Only one unpinning event is considered and it occurs from the precipitate pointed out in every configuration.

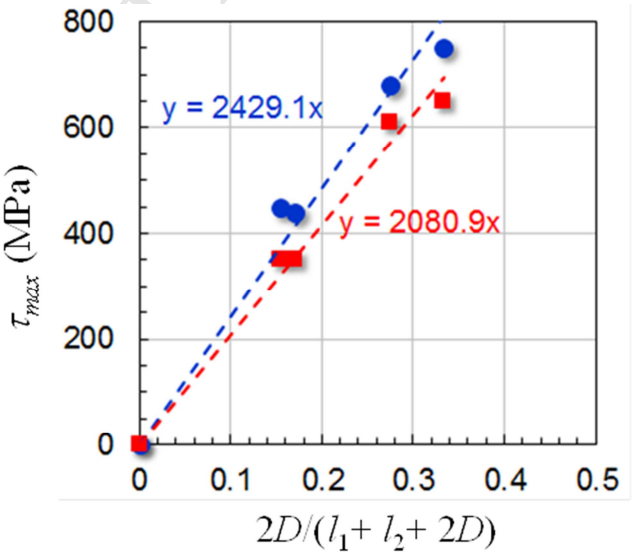

Figure 12: The unpinning stress as a function of the ratio $2D/(l_1 + l_2 + 2D)$. The slope provides the precipitate resistance. Circles refer to simulations at 300 K and rectangles to simulations at 600 K. (Segregation temperature: 500 and 550 K).

Of course, the decrease in the resistance is due to thermal activation, as was also reported in the case of Cr precipitates [22]. The specific values obtained from each simulation are given in Table 4.

Table 4: Precipitate resistance (MPa) computed from MD simulations of the different alloys at 300 and 600 K. (Segregation temperature: 500 and 550 K).

	600K	300K
1%Ni-1%Mn	2200	2500
0.7%Ni-0.8%Mn	2300	2900
0.7%Ni-2%Mn	2100	2600
0.5%Cu-1%Ni-1%Mn	2000	2300

The different values reported in Table 4 are of the same order of magnitude as those obtained for Cu and Cr precipitates in iron [22]. This seems to confirm that this order of magnitude is common to most coherent precipitates in iron. However, we must be careful in relating the precipitate resistance (on the order of 2.5 GPa) with the induced hardening (on the order of some tens to some hundreds of MPa). The former measures the friction stress *inside* the defects resisting to the shear of the precipitate by the dislocation, while the latter reflects the effect of precipitates on the overall collective behavior of dislocations, which depends on the precipitate size, distribution and density, in addition to the precipitate resistance. In the following we give an example of role of the shear resistance in estimating the macroscopic hardening. Recently, thanks to dislocation dynamics simulations, it has been shown [22] that the hardening $\Delta\tau$ induced by random distribution of precipitates can be given by:

$$\Delta\tau = \left(\frac{\tau_{obs}}{\tau_\infty} \frac{\ln 2\underline{D}}{\ln 2l} \right)^{3/2} \frac{\mu}{2\pi l} \ln(2l) \qquad (7)$$

where τ_∞ is a constant (equal to 4.5 GPa), μ the shear modulus, l the average free planner spacing and $\underline{D}$ the harmonic mean of the precipitate size D and l. All lengths in Eq. (7) are normalized by the norm of the Burgers vector (0.248 nm). For typical values of radiation defect size (3 nm) and a density of 10^{23} m^{-3} [23] the free average spacing is close to 55 nm. If these precipitates are considered impenetrable, i.e. $\tau_{obs} = \tau_\infty$ and Eq. (7) reduces to the Bacon et al expression [24]. The Orowan hardening thereby predicted is close to 100 MPa in shear stress which (with a Taylor factor of 2.7 [25]) yields a macroscopic hardening larger than 270

MPa. This value is much larger than the one frequently measured in experiments [23]. But if we consider τ_{obs} = 2.7 GPa (the average value of τ_{obs} at 300 K in Table 4), $\Delta\tau$ predicted by Eq. (7) is 47 MPa and the macroscopic hardening is approximately 127 MPa, which is much closer to the measured hardening in low copper RPV steels.

In the light of this interpretation, the results reported in Table 2 (segregation temperature: 300K) can be easily rationalized. Since segregation is *almost* homogeneous along the dislocation line, the length of free segments (l_1 and l_2) decreases drastically, as can be shown in Fig.2.*a* and *b*. According to Eq. (6), when l_1 and l_2 go to zero, τ_{obs} becomes close to the unpinning stress. Therefore, with quite small values of l_1 and l_2, the unpinning stresses reported in Table 2 must be close to and slightly below the values of precipitate resistances reported in Table 4. A quick look at the two tables confirms this conclusion. The case of the last alloy (0.5%Cu-1%Ni-1%Mn) is especially interesting. As can be shown in Fig.13, there is almost no segregation free dislocation segment. Segregation is almost uniform. Lengths l_1 and l_2 are therefore almost zero, which, according to our model, requires that the unpinning stresses for this alloy (2400MPa in loading at 300K and 2100MPa in loading at 600K) and precipitate resistances (2300MPa at 300K and 2000MPa at 600K) computed from Eq. (6) (at different segregation temperature) must be very close, which is in excellent agreement with the reported results. This conclusion confirms that precipitates forming at 300 K and at 500 or 550 K are of similar resistance; the distribution of precipitates along the dislocation line alters the precipitate resistance, that decrease slightly with increasing temperature (this is likely to be the consequence of the slight decrease in the shear modulus, i.e. the line tension of the dislocation, rather than the decrease of the resistance itself).

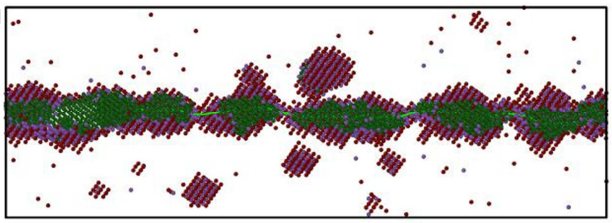

Figure 13: Configuration of solute segregation in the (0.5%Cu-1%Ni-1%Mn) obtained at 300K.

However, all the values of precipitate resistance reported in this work must not be considered as a unique indicator of hardening. Precipitate resistance is only one third of the story. As

shown earlier [22], hardening at the intragranular level is governed by three factors: the resistance, the average size and the density of precipitates. Given that most precipitates are of a few nm size and of resistance close to 2500 MPa, the precipitate density is probably the most important precipitation parameter for hardening. Effort must thus be made to characterize the distribution of the precipitate size in the different alloys.

The analysis of the case of the 0.5%Cu-1%Ni-1%Mn alloy applies also on the segregation of P along the dislocation line, since precipitation is almost uniform. The resistance of the phosphorous precipitates is thus almost equal to the maximum stress depicted in Fig.8.*b*. The resistance thus increases linearly with the P content in the alloys.

5. Summary and conclusions

We have simulated Cu, Ni, Mn and also P segregation/precipitation near a dipole of edge dislocations in a Fe matrix using an atomistic Monte Carlo (MC) method in the variance-constrained semi-grand-canonical (VC-SGC) ensemble. The results for Mn, Ni and Cu are fully consistent with the results already published by Bonny *et al*. [4,10], which were obtained with a different computational technique, thereby supporting their robustness. Subsequently, the effect of the segregation/precipitation on the mobility of the dislocation when a load is applied has been studied.

Based on the results obtained, segregation profiles and precipitates at the dislocation core act as strong obstacles for the edge dislocations. A B2 ordered phase formed by Ni and Mn appears to be especially hard, suggesting that alloys containing high amounts of these two elements, especially Ni that drives the precipitation of this phase, will be subjected to higher hardening. In contrast, since Cu reduces the amount of this phase that precipitates, overall it reduces the hardening effect. As a matter of fact, what mainly determines the hardening effect is the total amount of atoms that segregated or precipitated around the dislocation, as well as their distribution, in particular the distance between them along the dislocation line. The segregation temperature has an influence only insofar as it influences the amount of segregated atoms; however, it does not affect much the intrinsic precipitate resistance. This resistance has been estimated to be in average ~2400MPa at 300K and 2100MPa at 600K. These values can be directly used in larger scale simulations to estimate the hardening at the grain scale, given the precipitate distribution along the dislocation lines.

P strongly segregates to the edge dislocation core, to the compressive side of the dislocation field, without forming full-fledged precipitates. Still, the attractive binding energy leads to significant dislocation pinning. The resistance due to segregated P atoms seems to increase linearly with the P content, at least for small concentrations, the slope being close to the binding energy, as predicted by theory. For larger P contents, the curve deviates from linearity, probably because the P-P interactions are not taken into account in the cohesion model of the interatomic potential of the Fe-P used in our simulations.

Acknowledgements

One of the authors (M.I.Pascuet) thanks CONICET, Argentina and SCK•CEN, Belgium, for the accorded leave and hosting it, respectively. E.Martinez thanks LANL, an affirmative action/equal opportunity employer, operated by Los Alamos National Security, LLC, for the National Nuclear Security Administration of the U.S. DOE under contract DE-AC52-06NA25396. This project has received funding from the Euratom research and training programme 2014-2018 under grant agreement No 661913 (SOTERIA). This work also contributes to the Joint Program on Nuclear Materials (JPNM) of the European Energy Research Alliance (EERA).

References

[1] C. English, J.M. Hyde, 4.05 Radiation Damage of Reactor Pressure Vessel Steels, in: Comprehensive Nuclear Materials, Elsevier (2012).
[2] M.K. Miller, Russell, J. Nucl. Mat. 371 (2007) 145.
[3] M.K. Miller, K.A. Powers, R.K. Nanstad, P. Efsing, J. Nucl. Mat. 437 (2013) 107.
[4] G. Bonny, D. Terentyev, E.E. Zhurkin, L. Malerba, J. Nucl. Mat. 452 (2014) 486.
[5] D. Terentyev, X. He, G. Bonny, A. Bakaev, E. Zhurkin, L. Malerba, J. Nucl. Mat. 457 (2015) 173.
[6] Y. Nishiyama, T.E. Bloomer, J. Kameda, 2000 Microstructural Processes, Irradiated Materials Ed. G E Lucas, L L Snead, M A Kirk Jr and R G Elliman, (Pittsburgh, PA: Materials Research Society) p R6.10
[7] J.T. Buswell, C.J. Bolton, M.R. Wooton, P.E.J. Bischler, R.B. Jones, L.T. Jones, W.J. Phythian, R. Sinclair, 1993 Effects of Radiation on Materials (ASTM STP vol 1175) 332.
[8] S. Plimpton, J. Comp. Phys. 117 (1995) 1.
[9] B. Sadhig, P. Erhart, A. Stukowski, A. Caro, E. Martinez, L. Zepeda-Ruiz, Phys. Rev. B, 85 (2012) 184203.
[10] G. Bonny, D. Terentyev, A. Bakaev, E.E. Zhurkin, M. Hou, D. Van Neck, L. Malerba, J. Nucl. Mat. 442 (2013) 282.
[11] G.J. Ackland, M.I. Mendelev, D.J. Srolovitz, S. Han, A.V. Barashev, J. Phys.: Condens. Matter, 16 (2004) S2629–S2642.
[12] W. Cai, Md++. http://micro.standford.edu/MDpp/docs.
[13] E. Martinez, C.-C.Fu, Phys. Rev. B 84 (2011) 014203.
[14] D. Lidbury, E. Keim, B. Marini, L. Malerba, A. Zeghadi, D. Moinereau, A. Al Mazouzi, Overview of RPV Sub-Project of Perform 60, Paper No. PVP2011-57551, pp. 303-312; in: ASME 2011 Pressure Vessels and Piping Conference, Volume 6: Materials and Fabrication, Parts A and B, Baltimore, Maryland, USA, July 17–21, 2011.
[15] L. Messina, M. Nastar, T. Garnier, C. Domain, P. Olsson, Phys. Rev. B 90 (2014) 104203.
[16] Y.N. Osetsky, D.J. Bacon, Modelling Simul. Mater. Sci. Eng. 11 (2003) 427.
[17] A. Stukowski, K. Albe, Modelling Simul. Mater. Sci. Eng. 18 (2010) 085001.

[18] A. Stukowski, V.V. Bulatov, A. Arsenlis, Modelling Simul. Mater. Sci. Eng. 20 (2012) 085007.
[19] G. Monnet, in: I. Ionescu, S. Bouvier (Eds.), Plasticity of Crystalline Materials: from Dislocations to Continuum, ISTE Ltd., Hoboken, NJ, 2011, pp. 3–36.
[20] J.P. Hirth, J. Lothe and G. Monnet, Theory of Dislocations, Ed. Wiley, New York, 1982.
[21] G. Monnet, Y.N. Osetsky, D.J. Bacon, Phil. Mag. 90 (2010) 1001.
[22] G. Monnet, Acta Mat. 95 (2015) 302.
[23] C. English and J. Hyde, Radiation Damage of Reactor Pressure Vessel Steels, in: Comprehensive Nuclear Materials, Ed. Rudy J. M. Konings, 151‑80. Oxford: Elsevier, 2012.
[24] D.J. Bacon, U.F. Kocks and R.O. Scattergood, Phil. Mag. 28 (1973) 1241.
[25] J.M. Rosenberg and H.R. Piehler, Metallurgical Transactions 2 (1971) 257.